Article

# Monocopper Center Embedded in a Biomimetic Cavity: From Supramolecular Control of Copper Coordination to Redox Regulation

Nicolas Le Poul, Morgan Campion, Bndicte Douziech, Yannick Rondelez, Loc Le Clainche, Olivia Reinaud, and Yves Le Mest

*J. Am. Chem. Soc.*, **2007**, 129 (28), 8801-8810• DOI: 10.1021/ja071219h • Publication Date (Web): 20 June 2007



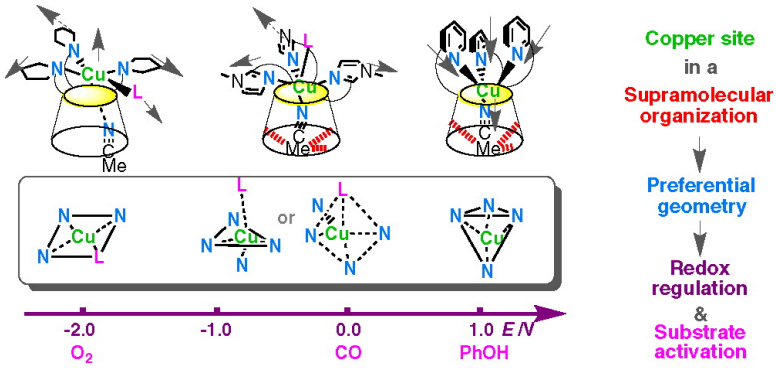


## More About This Article

Additional resources and features associated with this article are available within the HTML version:

- Supporting Information
- Links to the 3 articles that cite this article, as of the time of this article download
- Access to high resolution figures
- Links to articles and content related to this article
- Copyright permission to reproduce figures and/or text from this article

View the Full Text HTML

J|A|C|S
ARTICLES
Published on Web 06/20/2007

# Monocopper Center Embedded in a Biomimetic Cavity: From Supramolecular Control of Copper Coordination to Redox Regulation

Nicolas Le Poul,[†] Morgan Campion,[†] Bénédicte Douziech,[†] Yannick Rondelez,[‡] Loïc Le Clainche,[‡] Olivia Reinaud,[‡] and Yves Le Mest*,[†]

*Contribution from the Laboratoire de Chimie, Electrochimie Moléculaires et Chimie Analytique, UMR CNRS 6521, Université de Bretagne Occidentale, CS 93837, 6 avenue Le Gorgeu, 29238 Brest cedex 3, France, and Laboratoire de Chimie et Biochimie Pharmacologiques et Toxicologiques, UMR CNRS 8601, Université René Descartes-Paris 5, 45 rue des Saints Pères, 75270 Paris cedex 06, France*

Received February 20, 2007; E-mail: Yves.LeMest@univ-brest.fr

***Abstract:*** The electrochemical behavior of diversely substituted Cu-$N_3$-calix[6]arene, enzyme-like, "funnel" complexes is analyzed. The Cu(II)/Cu(I) redox process is regulated by the supramolecular organization of the Cu coordination. The presence of a "shoetree" alkyl nitrile guest molecule inside the host cavity is a prerequisite for a dynamic redox behavior. Combination of supramolecular CH$-\pi$ weak interactions with the calixarene cavity and electronic/steric effects from the $N_3$ substituting groups (pyridine, imidazole, pyrrolidine) enforces the preferential geometrical pattern adopted by Cu. This dictates the pathway of the electron-transfer process and, thus, the thermodynamics and kinetics of the redox reaction in the framework of a square-scheme mechanism. The present observations recall strongly the redox control exerted by the protein matrix on copper proteins through biological concepts such as induced fit mechanism, protein foldings, and entatic and allosteric effects.

## Introduction

Copper proteins and their low molecular weight synthetic models belong to the most studied metalloredox systems since the biological relevance and prevalence of copper has been fully recognized.[1−4] Through different types of coordination, the copper systems cover a large range of functionalities from "simple" electron transfer[2,3] to redox catalysis, most of them being involved in the metabolism of $O_2$.[4] In almost all processes, the functionality is based on the Cu(II)/Cu(I) electron exchange. Therefore, the knowledge of the factors governing their redox behavior is essential in regards to fundamental aspects and for the development of biomimetic devices.

The remarkable properties displayed by copper systems result from the specificity of the electronic and geometrical properties of this transition metal.[2,5] Cu(I) ($d^{10}$), due to its absence of crystal field, does not impose any force on the geometry of its environment and is generally found to afford four-coordinated tetrahedral (Td) geometries in an unconstrained environment. The crystal field force associated with a Jahn−Teller effect of the Cu(II) ($d^9$) ion tends to enforce a tetragonal geometry to its surrounding leading to either five-coordinate square-based pyramidal (SBP) complexes or six-coordinate octahedral and/or four-coordinate square-planar (SP) compounds. As a result, in unconstrained systems, Cu(II)/Cu(I) processes involve significant geometric rearrangements requiring important reorganization energies. In studies on electron-transfer kinetics for models of blue copper proteins, Rorabacher and co-workers have described the Cu(II)/Cu(I) processes in terms of a dual-pathway square-scheme mechanism in which conformational changes occur sequentially with the electron-transfer step (Scheme 1).[3,6−8] In this mechanism, O and R represent the oxidized and reduced stable species, respectively, whereas P and Q are metastable transient species. The geometries of O and P and

[†] Université de Bretagne Occidentale-Brest.
[‡] Université René Descartes-Paris 5.

(1) (a) Kaim, W.; Rall, J. *Angew. Chem., Int. Ed.* **1996**, *35*, 43−60. (b) Messerschmidt, A.; Huber, R.; Poulos, T.; Wieghardt, K. *Handbook of Metalloproteins*; Wiley, New York, 2001. (c) Karlin, K. D.; Tyeklàr, Z. Bioinorganic Chemistry of Copper; Chapman & Hall: New York, London, 1993.
(2) (a) Solomon, E. I.; Szilagyi, R. K.; George, S. D.; Basumallick, L. *Chem. Rev.* **2004**, *104*, 419−458. (b) Li, H.; Webb, S. P.; Ivanic, J.; Jensen, J. H. *J. Am. Chem. Soc.* **2004**, *126*, 8010−8019. (c) George, S. D.; Basumallick, L.; Szilagyi, R. K.; Randall, D. W.; Hill, M. G.; Nersissian, A. M.; Valentine, J. S.; Hedman, B.; Hodgson, K. O.; Solomon, E. I. *J. Am. Chem. Soc.* **2003**, *125*, 11314−11328. (d) Gray, H. B.; Malmström, B. G.; Williams, R. J. P. *J. Biol. Inorg. Chem.* **2000**, *5*, 551−559.
(3) Rorabacher, D. B. *Chem. Rev.* **2004**, *104*, 651−697.
(4) (a) Zhang, C. X.; Liang, H.-C.; Humphreys, K. J.; Karlin, K. D. In *Advances in Catalytic Activation of Dioxygen by Metal Complexes*; Simándi, L. I., Ed.; Kluwer Academic Publishers: Dordrecht, The Netherlands, 2003; pp 79−121. (b) Solomon, E. I.; Chen, P.; Metz, M.; Lee, S.-K.; Palmer, A. E. *Angew. Chem., Int. Ed.* **2001**, *40*, 4570−4590. (c) Mirica, L. M.; Ottenwaelder, X.; Stack, T. D. P. *Chem. Rev.* **2004**, *104*, 1013−1045. (d) Lewis, E. A.; Tolman, W. B. *Chem. Rev.* **2004**, *104*, 1047−1076. (e) Kim, E.; Chufán, E. E.; Kamaraj, K.; Karlin, K. D. *Chem. Rev.* **2004**, *104*, 1077−1133. (f) Itoh, S. *Curr. Opin. Chem. Biol.* **2006**, *10*, 115−122.
(5) (a) Hathaway, B. J.; Billing, D. E. *Coord. Chem. Rev.* **1970**, *5*, 143−207. (b) Hathaway, B. J. *Coord. Chem. Rev.* **1981**, *35*, 211−252. (c) Hathaway, B. J. *Struct. Bonding (Berlin)* **1984**, *57*, 55−118.
(6) Martin, M. J.; Endicott, J. F.; Ochrymowycz, L. A.; Rorabacher, D. B. *Inorg. Chem.* **1987**, *26*, 3012−3022.

***Scheme 1.*** Square-Scheme Mechanism As Proposed by Rorabacher et al. (Ref 3)

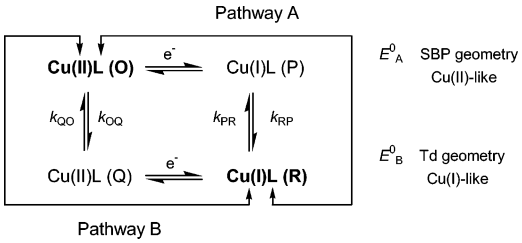


those of R and Q are thus SBP and Td, respectively.[9] Electron transfer operates through the most favorable route (pathway A or B) allowed by the most stable of the two metastable species. Hence, the classical route of electron transfer for Cu complexes is pathway A for which Cu(I) geometry is in an SBP−Td equilibrium due to its geometrical adaptability in an unconstrained environment. These authors first established that the presence of two anodic peaks on the Cu(II)/Cu(I) voltammograms corresponds to the oxidation of both P and R species under an equilibrium ($E^0_A < E^0_B$).[7] Most of the studies reported in the literature described such a route to rationalize the shape of CVs of Cu complexes. Very few examples of route B have been evidenced by using voltammetric methods.[8,10−13]

This mechanism is of exceptional interest for biological redox processes, since it experimentally evidenced the "gated electron-transfer" theory,[14] along which the conformational strains exerted by the protein matrix on the geometry of the redox site provide an ultimate control on the redox process. This concept coincides with the theory of the entatic "energized" state of Vallee and Williams,[15] corresponding to enhanced electronic properties resulting from the geometric constraints exerted by the embedding protein on the active sites.[16] These effects were proposed to apply to the efficiency of "simple" electron-transfer processes[2,3,17] and to the activation of substrates such as $O_2$.[18]

***Scheme 2.*** Representation of the Simplified Topological Reorganization Td/SBP at the Cu(II)/Cu(I) Redox Process for Cu-$N_3$-Calix[6]arene Complexes and XRD Structures of Complexes $[Cu^I N_3(EtCN)]^+$ and $[Cu^{II} N_3(MeCN)(H_2O)]^{2+}$ Stabilized by a Tris(pyridine) and a Tris(imidazole) Core, Respectively (Refs 19a−c)[a]

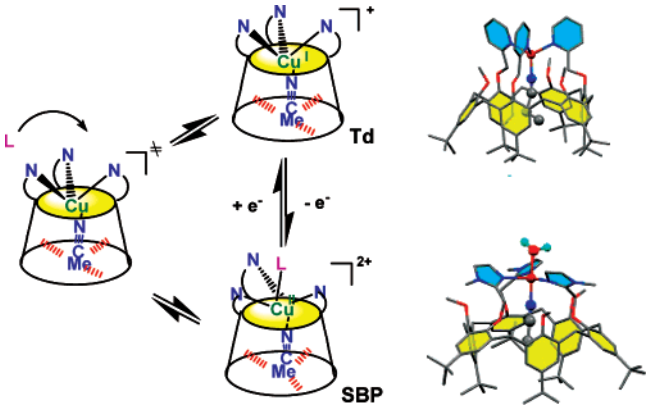


[a] Red lines symbolize CH−$\pi$ interactions.

These theories illustrate the important biological relevance of the Cu(II)/Cu(I) processes. In spite of this, very few thorough electrochemical studies of the topological organization of the Cu coordination have been developed.[7,10−13] An aspect which has never been unraveled so far, for low molecular weight synthetic models, is the effect exerted on the metal by a pocket surrounding the binding site although it refers to important issues such as the lock-and-key and induced fit concepts which define the protein/substrate relationship.[2,3,15−17] In this perspective, we have developed a supramolecular platform based on a calix[6]-arene cone functionalized by three independent N-donor groups leading, upon binding to copper, to the so-called funnel complexes (Scheme 2).[19−21] In a preliminary communication, we reported that the tris(pyridine)-calix[6]arene Cu complex displayed an unusual electrochemical behavior.[13] We proposed that the presence of MeCN inside the cavity, as a so-called "shoetree" molecule, was a prerequisite to a resolved electrochemical behavior and that the redox process was under control of a square-scheme mechanism. This was the first example of a Cu complex whereby the supramolecular control of the coordination by a protein-like pocket determines the dynamics

(7) (a) Bernardo, M. M.; Robandt, P. V.; Schroeder, R. R.; Rorabacher, D. B. *J. Am. Chem. Soc.* **1989**, *111*, 1224−1231. (b) Bernardo, M. M.; Schroeder, R. R.; Rorabacher D. B. *Inorg. Chem.* **1991**, *30*, 1241−1247. (c) Robandt, V.; Schroeder, R. R.; Rorabacher, D. B. *Inorg. Chem.* **1993**, *32*, 3957−3963. (d) Villeneuve, N. M.; Schroeder, R. R.; Ochrymowycz, L. A.; Rorabacher, D. B. *Inorg. Chem.* **1997**, *36*, 4475−4483.
(8) (a) Ambundo, E. A.; Yu, Q.; Ochrymowycz, L. A.; Rorabacher, D. B. *Inorg. Chem.* **2003**, *42*, 5267−5273. (b) Ambundo, E. A.; Ochrymowycz, L. A.; Rorabacher, D. B. *Inorg. Chem.* **2001**, *40*, 5133−5138. (c) Yu, Q.; Salhi, C. A.; Ambundo, E. A.; Heeg, M. J.; Ochrymowycz, L. A.; Rorabacher, D. B. *J. Am. Chem. Soc.* **2001**, *123*, 5720−5729.
(9) Several cases of Cu(II) complexes with $C_{3v}$ geometry have also been reported (see refs 3, 5, and 8).
(10) (a) Flanagan, S.; Dong, J.; Haller, K. H.; Wang, S.; Scheidt, W. R.; Scott, R. A.; Webb, T. R.; Stanbury, D. M.; Wilson, L. J. *J. Am. Chem. Soc.* **1999**, *119*, 8857−8868. (b) Xie, B.; Elder, T.; Wilson, L. J.; Stanbury, D. M. *Inorg. Chem.* **1999**, *38*, 12−19. (c) Xie, B.; Wilson, L. J.; Stanbury, D. M. *Inorg. Chem.* **2001**, *40*, 3606−3614.
(11) (a) Koshino, N.; Kuchiyama, Y.; Ozaki, H.; Funahashi, S.; Takagi, H. D. *Inorg. Chem.* **1999**, *38*, 3352−3360. (b) Koshino, N.; Kuchiyama, Y.; Funahashi, S.; Takagi, H. D. *Can. J. Chem.* **1999**, *77*, 1498−1507. (c) Itoh, S.; Funahashi, S.; Koshino, N.; Takagi, H. D. *Inorg. Chim. Acta* **2001**, *324*, 252−265. (d) Itoh, S.; Takagi, H. D. *Inorg. Chem. Commun.* **2002**, *5*, 949−953.
(12) Amatore, C.; Barbe, J.-M.; Bucher, C.; Duval, E.; Guilard, R.; Verpeaux, J.-N. *Inorg. Chim. Acta* **2003**, *356*, 267−278.
(13) Le Poul, N.; Campion, M.; Izzet, G.; Douziech, B.; Reinaud, O.; Le Mest, Y. *J. Am. Chem. Soc.* **2005**, *127*, 5280−5281.
(14) (a) Hoffman, B. M.; Ratner, M. A. *J. Am. Chem. Soc.* **1987**, *109*, 6237−6243. (b) Brunschwig, B. S.; Sutin, N. *J. Am. Chem. Soc.* **1989**, *111*, 7454−7465.
(15) (a) Vallee, B. L.; Williams, R. J. P. *Proc. Natl. Acad. Sci. U.S.A.* **1968**, *59*, 498−505. (b) Williams, R. J. P. *Eur. J. Biochem.* **1995**, *234*, 363−381. (c) Williams, R. J. P. *Inorg. Chim. Acta Rev.* **1971**, 137−155.
(16) (a) Comba, P. *Coord. Chem. Rev.* **1999**, *182*, 343−371. (b) Comba, P. *Coord. Chem. Rev.* **2000**, *200*, 217−202. (c) Comba, P.; Schiek, W. *Coord. Chem. Rev.* **2003**, *238−239*, 21−29.
(17) Mbofana, C.; Zimmer, M. *Inorg. Chem.* **2006**, *45*, 2598−2602.
(18) (a) Börzel, H.; Comba, P.; Hagen, K. S.; Katsichis, C.; Pritzkow, H. *Chem. Eur. J.* **2000**, *6*, 914−919. (b) Börzel, H.; Comba, P.; Hagen, K. S.; Kerscher, M.; Pritzkow, H.; Schatz, M.; Schindler, S.; Walter, O. *Inorg. Chem.* **2002**, *41*, 5440−5452.
(19) (a) Blanchard, S.; Le Clainche, L.; Rager, M.-N.; Chansou, B.; Tuchagues, J.-P.; Duprat, A. F.; Le Mest, Y.; Reinaud, O. *Angew. Chem., Int. Ed.* **1998**, *37*, 2732−2735. (b) Le Clainche, L.; Rondelez, Y.; Sénèque, O.; Blanchard, S.; Campion, M.; Giorgi, M.; Duprat, A. F.; Le Mest, Y.; Reinaud, O. *C. R. Acad. Sci., Ser. IIc, Chim.* **2000**, *3*, 811−819. (c) Le Clainche, L.; Giorgi, M.; Reinaud, O. *Inorg. Chem.* **2000**, *39*, 3436−3437. (d) Rondelez, Y.; Sénèque, O.; Rager, M.-N.; Duprat, A. F.; Reinaud, O. *Chem. Eur. J.* **2000**, *6*, 4218−4226. (e) Rondelez, Y.; Rager, M.-N.; Duprat, A. F.; Reinaud, O. *J. Am. Chem. Soc.* **2002**, *124*, 1334−1340. (f) Rondelez, Y. Ph. D. Thesis, Universit'e Paris XI, 2002. (g) Le Clainche, L. Ph. D. Thesis, Université Paris VI, 2000. (h) Sénèque, O.; Rondelez, Y.; Le Clainche, L.; Inisan, C.; Rager, M.-N.; Giorgi, M.; Reinaud, O. *Eur. J. Inorg. Chem.* **2001**, 2597−2604.
(20) Two other generations of calix[6]arene ligands have been synthesized since. For the most recent, the calix-aza-cryptand ligands display covalently bound functional groups, and the metal is totally entrapped leading to an almost blocked trigonal geometry for Cu. See: (a) Izzet, G.; Douziech, B.; Prangé, T.; Thomas, A.; Jabin, I.; Le Mest, Y.; Reinaud, O. *Proc. Natl. Acad. Sci. U.S.A.* **2005**, *102*, 6831−6836. (b) Izzet, G.; Xeng, X.; Douziech, B.; Zeitouny, J.; Giorgi, M.; Jabin, I.; Le Mest, Y.; Reinaud, O. *Inorg. Chem.* **2007**, *46*, 375−377.
(21) Reinaud, O.; Le Mest, Y.; Jabin, I. In *Calixarenes in the Nanoworld*; Harrowfield J., Vicens, J., Eds.; Springer: Dordrecht, The Netherlands, 2006; Chapter 13.

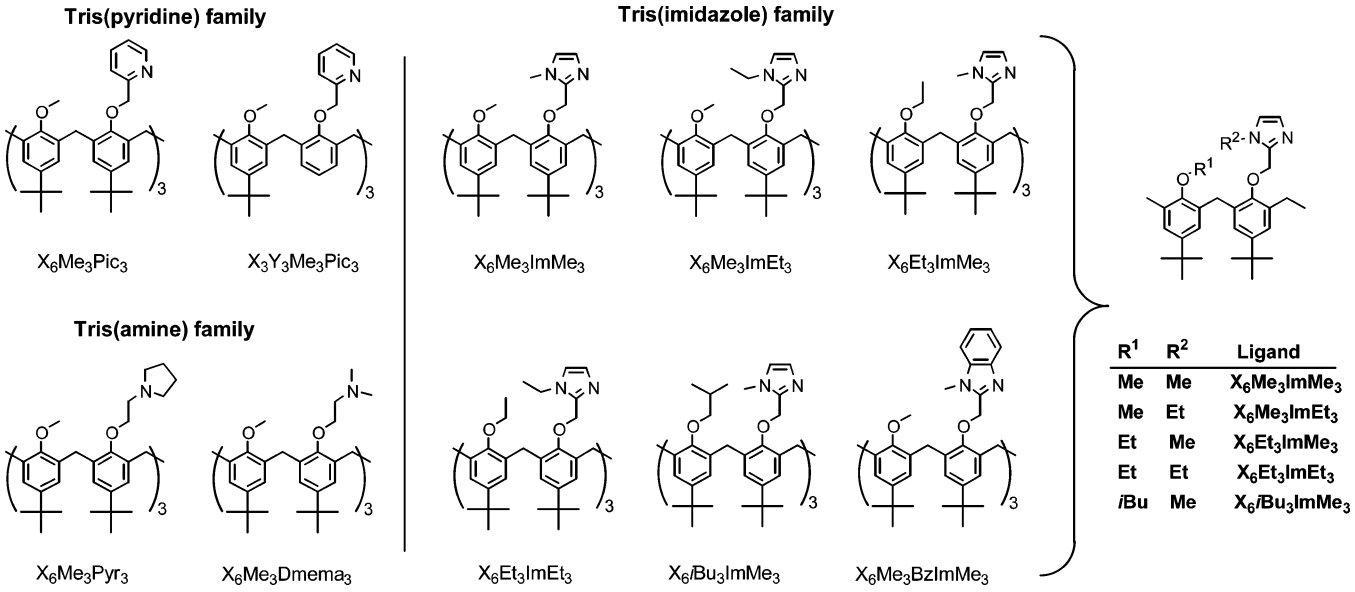


***Figure 1.*** Representation and denomination of the three families of the $N_3$-calix[6]arene ligands.

***Table 1.*** Electrochemical Data [$E_{1/2}$/V vs Fc ($\Delta E_p$/mV)] for the Cu-$N_3$-Calix[6]arene Complexes in MeCN[a]

| complex | $E_{1/2}$/V ($\Delta E_p$/mV) | synthesis and characterization (refs) |
|---|---|---|
| $[Cu^I(X_6Me_3Pic_3)]^+$ | +0.50 (500) | $Cu^I$ (19a), $Cu^{II}$ (19b) |
| $[Cu^I(X_3Y_3Me_3Pic_3)]^+$ | $E_{pa}$ (irr) = +0.90 | $Cu^I$ (19e) |
| $[Cu^I(X_6Me_3ImMe_3)]^+$ | +0.06 (400) | $Cu^I$ (19d,f), $Cu^{II}$ (19c) |
| $[Cu^I(X_6Me_3ImEt_3)]^+$ | +0.09 (500) | $Cu^I$ (19d,f), $Cu^{II}$ (19c) |
| $[Cu^I(X_6Et_3ImMe_3)]^+$ | +0.01 (150) | $Cu^I$ (19d,f) |
| $[Cu^I(X_6Et_3ImEt_3)]^+$ | +0.02 (600) | $Cu^I$ (19d) |
| $[Cu^I(X_6iBu_3ImMe_3)]^+$ | +0.01 (100) | $Cu^I$ (19f) |
| $[Cu^I(X_6Me_3BzImMe_3)]^+$ | +0.20 (90) | $Cu^I$ (19g) |
| $[Cu^{II}(X_6Me_3Pyr_3)]^{2+}$ | $E_{pc}$ (irr) = −1.60 | $Cu^I$ (19g) |
| $[Cu^{II}(X_6Me_3Dmema_3)]^{2+}$ | $E_{pc}$ (irr) = −1.22 | $Cu^I$ (19g) |

[a] Recorded at 0.1 V $s^{-1}$ at a Pt electrode in MeCN/$NBu_4PF_6$. Similar values were obtained with the Cu(II) complexes, when available.

of electron transfer. Moreover, the redox pathway proposed as B (Scheme 1) led us to conclude that the highly oxidizing Cu(II) Td state corresponds to a definitive example of a real entatic state.[13,15]

In the present article, we have extended this work to three families of Cu-$N_3$-calix[6]arene complexes (Figure 1) in order to evaluate the factors which affect the topological reorganization when the electron exchange is involved, and thereby the structural effects of ligands on the redox properties: (i) cone size for the pyridine-based calixarene; (ii) electronic effects exerted by different electrodonating N-ligands; (iii) steric crowding on the top of the cone on diversely substituted imidazole derivatives. The present results emphasize novel concepts in terms of redox regulation through supramolecular control of the coordination of Cu, relevant to metal in a biological environment.

## Results

The various ligands used in the present studies are depicted in Figure 1, and references to their Cu complexes are given in Table 1. The unique topology of this first generation of ligands, upon binding to copper, constrains the metal inside the cone configuration of the calix[6]arene and preserves a binding site, accessible to small exogenous ligands, deeply entrapped inside the enzyme-like pocket.[19−21] All characterization studies (NMR, EPR, UV−vis, XRD) demonstrated that these funnel complexes are exemplary supramolecular structural models for monocopper enzyme active sites. As emphasized in Scheme 2, the global architecture of the system is best ensured by a small alkyl nitrile molecule inside the cavity through concurrent participations of Cu−nitrile bonding and CH−$\pi$ interactions between the alkyl group of the nitrile and phenyl units of the cavity.[19a−c] Cu(I) is stabilized in the classical Td configuration, whereas Cu(II) adopts the typical SBP geometry, slightly distorted, through the binding of an extra exogenous ligand ($H_2O$) at the upper access. In solution, for both redox states, the hydrophobic protein-like pocket of the calixarene controls the exchangeable guest, whose affinity depends on hard/soft characters of Cu(II) and Cu(I) ions, respectively. Cu(II) systems are receptive for various exogenous organic molecules such as nitriles, amides, alcohols, and water. Cu(I) complexes are insensitive to O-donors (including water), and they are also resistant to air oxidation in spite of their labile site. This stands in contrast to the classical model systems that undergo fast dimerization into Cu(II) dinuclear complexes upon exposure to dioxygen.[4]

**Electrochemical Behavior.** The electrochemical behavior of the Cu(I) and Cu(II) complexes of the calix[6]arene ligands depicted in Figure 1 has been examined in a series of noncoordinating ($CH_2Cl_2$, THF) and coordinating (MeCN, PhCN) solvents under an inert atmosphere ($N_2$) glovebox ($O_2$ < 1 ppm, $H_2O$ < 1 ppm). In noncoordinating solvents, the results for both Cu(II) and Cu(I) complexes cannot be interpreted except for the tris(pyrrolidine) compound. For a purpose of clarity, the observations in those media are presented in the Supporting Information. Actually, the electrochemical behavior of the copper complexes could only be resolved and analyzed in MeCN. This behavior can be classified into three categories corresponding to the three families of ligands (Figure 1) for which comparative cyclic voltammograms (CV) are presented in Figure 2. Electrochemical data are gathered in Table 1. The comparative behavior of both Cu(I) and Cu(II) compounds which did not reveal major differences is also presented in the Supporting Information. The redox mechanisms have been elucidated by cyclic voltammetry at different scan rates ($\upsilon$).

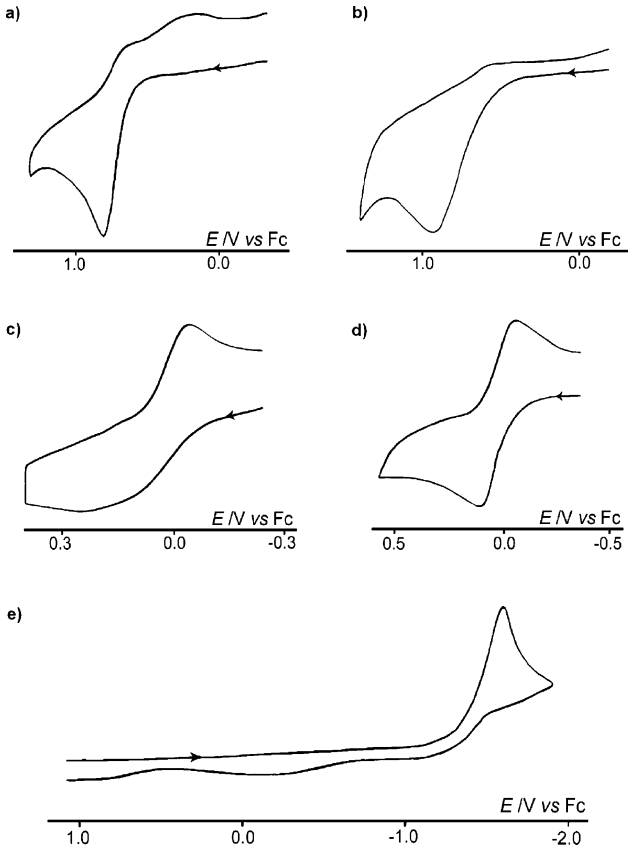


***Figure 2.*** Cyclic voltammetry at a Pt electrode in MeCN under $N_2$ of (a) $[Cu^{I}(X_6Me_3Pic_3)]^+$, (b) $[Cu^{I}(X_3Y_3Me_3Pic_3)]^+$, (c) $[Cu^{I}(X_6Me_3ImMe_3)]^+$, (d) $[Cu^{I}(X_6iBu_3ImMe_3)]^+$, and (e) $[Cu^{II}(X_6Me_3Pyr_3)]^{2+}$. Supporting salt: $NBu_4PF_6$; $v = 0.1$ V $s^{-1}$.

**Tris(pyridine) Complexes and Size of the Host Cone at the Large Rim.** The CV of the $[Cu^{I}(X_6Me_3Pic_3)]^+$ complex in MeCN (Figure 2a) and that of the Cu(II) derivative (Supporting Information Figure SI1) display the same features with a clearly resolved anodic peak at $E_{pa} = +0.8$ V associated to a broad cathodic process, emphasizing two peaks at ca. +0.5 and +0.2 V. The two complexes can be interconverted by electrolysis (1 $e^-$ exchange). The spectral and electrochemical characteristics of the generated redox states establish the full chemical reversibility of the process. In PhCN (Supporting Information Figure SI1), broad and totally irreversible peaks are observed for the Cu(I) and Cu(II) compounds. Electrolyses resulted in the appearance of the oxidized or reduced species, as indicated by voltammetry and spectroscopy, but required a very long time scale (20−30% after 3−4 h). This can be related to a chemically reversible and very slow process. Thus, as previously proposed, the most noteworthy point of this study is the presence of the small nitrile as the prerequisite for the observation of a Cu(II)/Cu(I) electrochemical interconversion,[22] whereas the bulkier PhCN guest, which was shown to distort the $X_6Me_3Pic_3$ cone,[19e] leads to a slowing down of the redox process. In order to corroborate the previous conclusion about the role of the CH−$\pi$ weak interactions and the influence of the size and flexibility of the cone on electrochemical data,[13] we have compared the redox behavior of the $[Cu^{I}(X_3Y_3Me_3Pic_3)]^+$ complex to that of $[Cu^{I}(X_6Me_3Pic_3)]^+$ one in MeCN (Figure 2, parts b and a). Indeed, the removal of three *t*Bu substituents at the large rim results in an enlarged and more open cavity with a 100-fold increase of the MeCN exchange rate for the tris(pyridine)Cu(I) complex (dissociative process) as shown by $^1$H NMR spectroscopy and modeling studies.[19e] Interestingly, the $[Cu^{I}(X_3Y_3Me_3Pic_3)]^+$ complex is characterized by an irreversible oxidation in MeCN (Supporting Information Figure SI2), contrarily to the $[Cu^{I}(X_6Me_3Pic_3)]^+$ cation. This indicates that the structural reorganization at the electron exchange site becomes ill-controlled. It seems that the interactions of *Me*CN with the larger cavity of $X_3Y_3Me_3Pic_3$ are not strong enough to allow reversibility. As depicted in Scheme 3, this clearly demonstrates that the size and flexibility of the calix[6]arene cavity must be sufficiently adapted to the structure of the guest nitrile ligand in order to stabilize the geometry of the copper ion, not only in both of its stable redox states, but also in the intermediate transient species (Scheme 2). Consequently, this adaptive process is necessary to observe Cu(II)/Cu(I) reversible redox processes in a dynamic mode. This behavior is similar to that of enzymes whose functionality is governed by the ability for the host proteic cavity to adapt to and to enclose the guest substrate.

***Scheme 3.*** Illustration of the Effect of the Calixarene Substitution at the Large Rim (Ref 19e)[a]

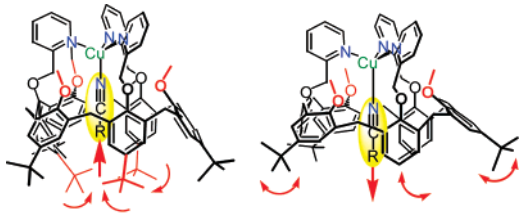


[a] Left: the *in t*Bu substituents close the cavity entrance, thereby strengthening the guest trapping. Right: their removal opens the cavity and increases its flexibility, thereby weakening the guest trapping.

**Tris(imidazole) Complexes and Influence of −OR$^1$ and −NR$^2$ Substituents at the Small Rim.** The interest of the tris(imidazole) derivatives stems from the fact that they are the most "biomimetic" as the imidazole substituent corresponds to the histidine residues found in proteic environment. The biological relevance of the tris(imidazole) calix[6]arene copper complexes has been clearly emphasized by their structural features and behavior.[21] Moreover, this ligand core offers the possibility to explore the impact of steric crowding at the top of the calixarene cone by varying $R^1$ and $R^2$ groups at the −OR$^1$ phenoxo and −NR$^2$ imidazole moieties, respectively (Figure 1). At last, imidazole has a stronger electron-donating power than pyridine. The generic ligand of the series is the bis(methyl) derivative with $R^1 = R^2 =$ Me, i.e., $X_6Me_3ImMe_3$. It is the less sterically hindered and thus the most adapted for comparison with other families. The CV of the $[Cu^{I}(X_6Me_3ImMe_3)]^+$ cation in MeCN is presented in Figure 2c. It shows a broad anodic peak at ca. 0.2 V associated with a well-defined cathodic peak at −0.1 V. The same pattern is observed for $[Cu^{II}(X_6Me_3ImMe_3)]^{2+}$. The two redox states can be interconverted by electrolysis (1 $e^-$). In PhCN, the $[Cu^{I}(X_6Me_3ImMe_3)]^+$ complex

(22) A similar behavior has been reported in the rare cases of Cu complexes in a hydrophobic environment. See: (a) Carrier, S. M.; Ruggiero, C. E.; Houser, R. P.; Tolman, W. B. *Inorg. Chem.* **1993**, *32*, 4889−4899. (b) Jonas, R. T.; Stack, T. D. P. *Inorg. Chem.* **1998**, *37*, 6615−6629. (c) Kuzelka, J.; Mukhopadhyay, S.; Spingler, B.; Lippard, S. J. *Inorg. Chem.* **2004**, *43*, 1751−1761.

displays a very broad anodic peak at ca. +0.7 V. The CV recorded after its slow electrolytic oxidation shows a broad cathodic peak at ca. −0.2 V, similar to the Cu(II) derivative redox features. Hence in PhCN, again only a very slow Cu(II)/Cu(I) process is observed. The trends in regards to the solvent effect on the shape of this CV are close to that observed with the tris(pyridine), since the presence of MeCN is again necessary for the observation of a pseudoreversible process (Supporting Information Figure SI3).[23] However, in comparison to the tris(pyridine) derivative, a reversed pattern is observed with a well-defined reduction peak and a composite oxidation peak, which corresponds to the CV features observed for the classical pathway A (Scheme 1).[3,7] This is in agreement with the spectroscopic studies which showed that, in contrast with the tris(pyridine) derivative, the tris(imidazole) system stabilizes Cu(II) in an SBP geometry[19c] but gives conformationaly ill-defined Cu(I) complexes, except in the presence of a strong $\pi$-acceptor such as CO.[19d]

The behavior of MeCN solutions of the complexes of diversely substituted (tris)imidazole ligands, $[Cu^{I}(X_6R^1{}_3ImR^2{}_3)]^+$, emphasizes the impact of steric hindrance on the voltammetric shape. With the less bulky $R^1$ groups ($R^1$ = Me), the CVs of the complexes, such as $[Cu^{I}(X_6Me_3ImMe_3)]^+$ (Figure 2c), reveal a slow reorganization for the oxidation of the Cu(I) derivative displaying a broad anodic peak and a large peak separation $\Delta E_p$ (Table 1). Remarkably, for each compound having bulkier $-OR^1$ or $-NR^2$ groups (Et, *i*Bu) or for the tris(benzimidazole) derivative, the CVs for the Cu(II)/Cu(I) process reach more closely the reversibility. They display both well-defined cathodic and anodic peaks with a lower $\Delta E_p$ and $i_{pa}/i_{pc} \approx 1$, as shown in Figure 2d for $[Cu^{I}(X_6iBu_3ImMe_3)]^+$. Similar observations are obtained for the $[Cu^{I}(X_6Et_3ImMe_3)]^+$ and $[Cu^{I}(X_6Me_3BzImMe_3)]^+$ hindered complexes (Table 1). This suggests a less important and/or faster coordination rearrangement at the electron exchange. The electrochemical behavior of the tris(imidazole) complexes can thus be rationalized in terms of steric hindrance at the small rim of the calix[6]arene cone.[19c,d] With nonhindered small rims, the system is highly mobile and flexible,[24] leaving the Cu free to reorganize its coordination at the electron exchange (Scheme 4, top). Conversely highly bulky $-OR^1$ and $-NR^2$ groups strongly reject the corresponding large rim *t*Bu substituents inside the cavity[24] and tend to rigidify the overall conformation of the system at either redox state (Scheme 4, bottom).

**Tris(amine) Complexes.** For comparison with the other N-donor ligands, the influence of a cyclic amine, the pyrrolidine, has been examined (Figure 1). The tris(pyrrolidine) tagged-cone $X_6Me_3Pyr_3$ ligand is a bulkier and stronger donor. The Cu(II) complex $[Cu^{II}(X_6Me_3Pyr_3)(H_2O)_2](OTf)_2$ displays an SBP structure, and its redox behavior has been compared to that of the Cu(II) derivative of a noncyclic and less hindered tertiary amine substituted ligand, the tris(dimethylamine) $X_6Me_3Dmema_3$ (Figure 1). For both ligands, several attempts to isolate the Cu(I) derivative failed. Moreover, Cu(I)/ligand mixtures displayed

***Scheme 4.*** Effect of the Calixarene Substitution at the Small Rim[a]

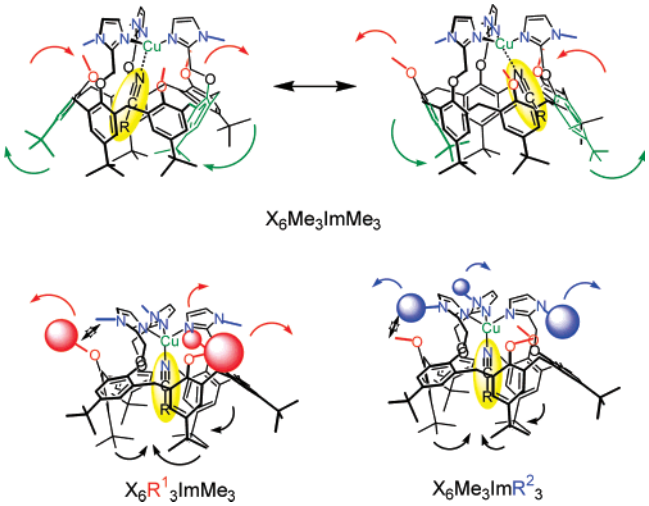


[a] The small −OMe and −NMe substituents confer to the calixarene structure a large flexibility (top) compared to that of ligands having larger $-OR^1$ groups or $-NR^2$ groups (bottom) (ref 24).

high reactivity toward $O_2$, whereas Cu(I) derivatives of the other families are insensitive to $O_2$.[25] The voltammograms of the $[Cu^{II}(X_6Me_3Pyr_3)]^{2+}$ complex have been recorded in MeCN (Figure 2e), and comparison in $CH_2Cl_2$, THF, and PhCN is shown in Supporting Information Figure SI4. In contrast to the tris(pyridine) and the tris(imidazole) compounds, this complex displays essentially the same redox behavior in all solvents. Only a totally irreversible cathodic peak at −1.6 V is observed; it corresponds to a one-electron reduction of Cu(II) at the time scale of CV (Figure 2e). No anodic peak could be detected on the reverse scan (vide infra). Holding the scan at a potential value lower than the reduction peak led to the deposition of Cu(0) onto the surface of the electrode, as indicated by an anodic redissolution peak. Bulk electrolyses and coulometry, even at low temperature, led also to reduction by a two-electron exchange from Cu(II) to Cu(0). The redox behavior in MeCN of the $[Cu^{II}(X_6Me_3Dmema_3)]^{2+}$ complex is similar giving an irreversible cathodic peak, at a less negative potential (−1.2 V). This is probably due to a donor effect of the dimethylamine weaker than that of pyrrolidine.[26] In comparison to the two other families of complexes, the tris(amine) derivatives display very negative reduction potentials consistent with the stronger $\sigma$-donor character of these N functions.

**Experimental and Simulated Voltammetry in MeCN at Different Scan Rates: Redox Mechanisms.** The comparative behavior in MeCN for the different families of complexes clearly showed that the shape of the CVs and hence the redox mechanisms are strictly governed by the nature of the $N_3$-calix[6]arene ligand and are related to the presence of the MeCN "shoetree" molecule.[13] The next step was the determination of the reaction pathway of the Cu(II)/Cu(I) electron-transfer processes in MeCN for each family of complexes with the aim to understand the role played by the supramolecular organization of the Cu coordination. In the case of tris(pyridine) and tris(imidazole) compounds, the same procedure has been followed

(23) In some cases, especially for the Cu(I) compound, a second system can be observed at a higher potential of ca. +0.8 V, but this system is irreproducible in intensity. It is attributed to partial decomplexation which has been emphasized by NMR studies. See ref 19e.

(24) The impact of the nature of the $-OR^1$ and $-NR^2$ substituents on the conformation and flexibility of the calixarene structure for the different complexes has been the subject of detailed NMR and modeling studies on $Cu^{I}CO$ complexes. See ref 19d.

(25) The high reactivity of the transient instable Cu(I) species towards $O_2$ has been emphasized by a very high sensitivity of the CVs to the presence of $O_2$ at a very low partial pressure.

(26) The p$K_a$'s of pyrrolidine and tris(methyl)amine are, respectively, 11.27 and 9.10.

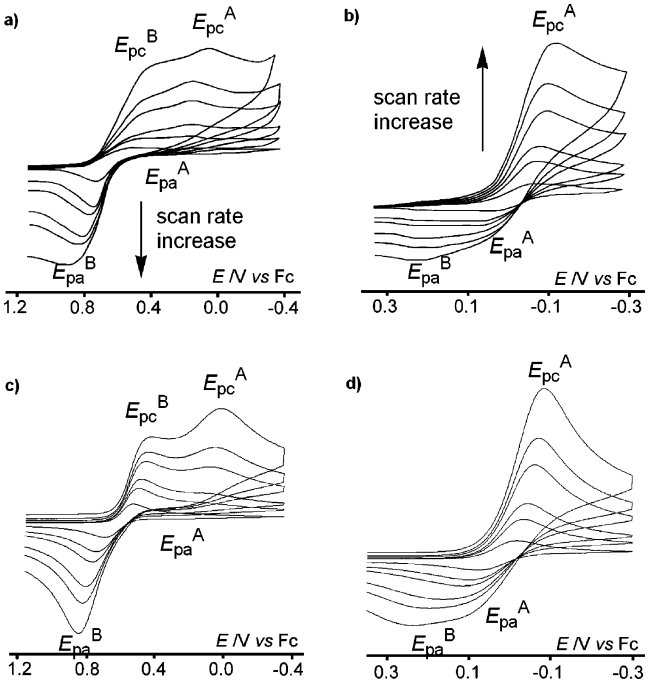


***Figure 3.*** Experimental (top) and simulated (bottom) CVs at different scan rates ($0.01 < v < 1$ V s$^{-1}$) of $[Cu^{II}(X_6Me_3Pic_3)]^{2+}$ (Panels a and c, respectively) and $[CuII(X_6Me_3ImMe_3)]^{2+}$ (Panels b and d, respectively) in MeCN, at a Pt electrode under $N_2$. Supporting salt: $NBu_4PF_6$.

***Scheme 5.*** Dual-Pathway Square-Scheme Mechanism for the Cu-$N_3$-Calix[6]arene Complexes in MeCN (Adapted from Ref 3): Representation of the Two Microscopic Redox Processes Associated with the Topological Reorganization

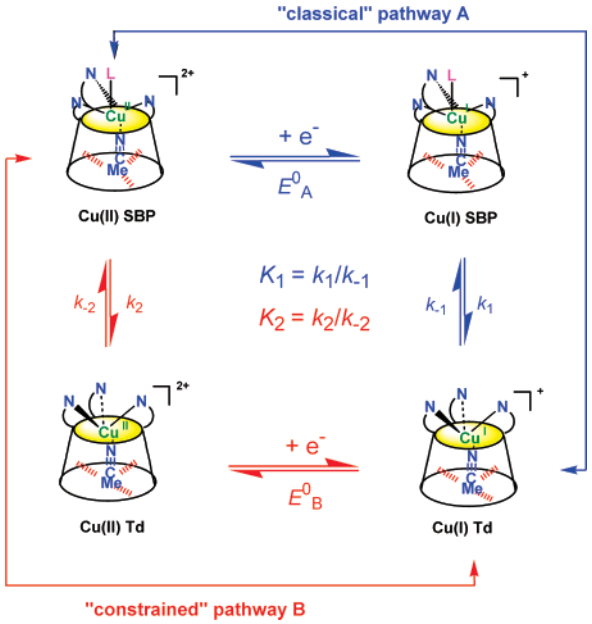


as in our preliminary report:[13] cyclic voltammetry at variable scan rates ($0.01 < v < 1$ V s$^{-1}$) was analyzed by Digisim simulation in the framework of a square-scheme SBP ↔ Td mechanism (Figure 3). It was adapted from Rorabacher's mechanism[3] (Scheme 1) to the Cu $N_3$-calix[6]arene complexes (Scheme 2) leading to Scheme 5. The kinetic and thermodynamic parameters obtained from the data fittings are listed in Table 2. For the hindered tris(imidazole) compounds, reversible systems have been obtained, and for the tris(amine) only the total irreversibility is observed. Thus, in these cases, no fitting

***Table 2.*** Kinetic and Thermodynamic Constants Obtained by Fitting Experimental CVs of Cu-$N_3$-Calix[6]arene Complexes by Digisim

| parameters | $X_6Me_3Pi_{c3}$ | $X_6Me_3ImMe_3$ |
|---|---|---|
| $E^0_A$/V vs Fc | +0.26(0) | +0.00(5) |
| $k^0_A$/cm s$^{-1}$ | $1.0 \times 10^{-3}$ | $2.0 \times 10^{-3}$ |
| $E^0_B$/V vs Fc | +0.65(0) | +0.16(0) |
| $k^0_B$/cm s$^{-1}$ | $1.0 \times 10^{-3}$ | $1.5 \times 10^{-3}$ |
| $K_1$ | $8 \times 10^5$ | 1.7 |
| $k_1$/s$^{-1}$ | $2.0 \times 10^4$ | 4.3 |
| $k_{-1}$/s$^{-1}$ | 0.025 | 2.5 |
| $K_2$ | 0.16 | $4.1 \times 10^{-3}$ |
| $k_2$/s$^{-1}$ | 11.2 | 367 |
| $k_{-2}$/s$^{-1}$ | 70 | $8.9 \times 10^4$ |

of the experimental CVs could be performed, and alternative mechanisms are proposed. Figure 3a displays the experimental CVs of the $[Cu^{II}(X_6Me_3Pic_3)]^{2+}$ dicationic complex at different scan rates. At low scan rates, a quasi-reversible system is observed at $E^0_B = +0.65$ V, $\Delta E_p = 300$ mV. As $v$ is increased, the anodic part of the CV becomes broad, while the reduction cathodic peak remains well-defined. A cathodic peak appears at $E_{pc}^A = +0.20$ V, becoming predominant over the peak at $E_{pc}^B = +0.50$ V. Such situation reveals the existence of an equilibrium in solution ($C_{rev}E$ process) at the Cu(II) redox state. A fourth peak at $E_{pa}^A \approx +0.3$ V, corresponding to the reverse peak of $E_{pc}^A$, is detected only at higher scan rates ($v > 1$ V s$^{-1}$) as it is the usual case with that kind of systems.[3,7] The behavior of the Cu(I) complex is equivalent to that of the Cu(II) one.[13] The intensity of the anodic peak $i_{pa}^B$ is linear with $v^{1/2}$, and on starting from the Cu(I) complex, the peak at $E_{pa}^A$ could not be detected even at very low scan rates: this indicates the absence of a CE process. As shown in Figure 3c, the CVs can be simulated with a satisfactory fit. The resulting thermodynamic ($K_1 = k_1/k_{-1} = 8 \times 10^5$) and kinetic ($k_1 = 2 \times 10^4$ s$^{-1}$) parameters indicate a high instability of the Cu(I) ion in the SBP conformation with fast conversion into the Cu(I) Td conformation (Scheme 5). This was also evidenced by the absence of the oxidation peak $E_{pa}^A$. On the other hand, the value obtained for the thermodynamic constant $K_2$ ($K_2 = k_2/k_{-2} = 0.16$) shows that the two geometries, Td and SBP, of the Cu(II) complex can coexist in equilibrium, the latter being slightly more stable. This is characterized by the presence of two reduction peaks ($E_{pc}^A$ and $E_{pc}^B$) at high scan rates on the experimental CVs. This behavior corresponds to the unclassical route B mechanism, in which Cu(I) is strongly stabilized in a Td environment and has lost its conformational adaptability. Instead the crossing of geometries (SBP ↔ Td) is observed for Cu(II) during the electron transfer.

As for the $[Cu^{II}(X_6Me_3ImMe_3)]^{2+}$ ion, Figure 3b emphasizes the strong effect of the N ligand, comparatively with the $[Cu^{II}(X_6Me_3Pic_3)]^{2+}$ compound: the situation is reversed back to the classical situation. At any scan rate, a single well-defined reduction peak at $E_{pc}^A = -0.10$ V is observed. Its peak current is a linear function of the square root of the scan rate, indicating that the cathodic reaction is limited by the diffusion of a Cu(II) species and not affected by a CE mechanism. The ill-defined shape of the CV (function of the scan rate) is now in the anodic part, with two convoluted oxidation peaks at $E_{pa}^A \approx +0.1$ V and $E_{pa}^B \approx +0.2$ V. For $v < 0.1$ V s$^{-1}$, the peak at $E_{pa}^A$ is predominant, but an increase of $v$ favors the appearance of the second oxidation peak at $E_{pa}^B$. This indicates that the two species in equilibrium at the Cu(I) redox state can be detected. An

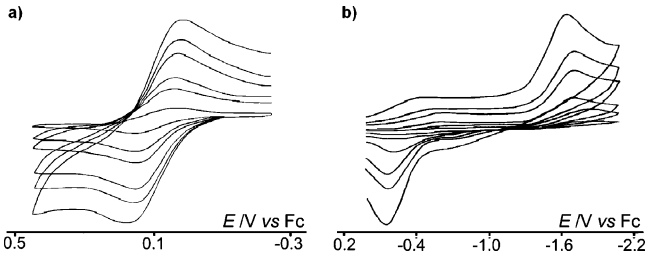


***Figure 4.*** Cyclic voltammetry of (a) $[Cu^{I}(X_6tBu_3ImMe_3)]^+$ and (b) $[Cu^{II}(X_6Me_3Pyr_3)]^{2+}$ in MeCN at a Pt electrode under $N_2$ at different scan rates ($0.01 < v < 1$ V $s^{-1}$). Supporting salt: $NBu_4PF_6$.

***Scheme 6.*** Representation of the Steric Effect on the Conformation of the Cone and Proposition of Redox Mechanism for the Complex $[Cu^{I}(X_6tBu_3ImMe_3)]^+$ in MeCN

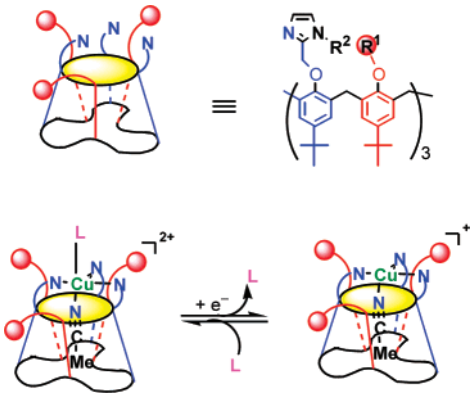

equivalent redox behavior was obtained with the $[Cu^{I}(X_6Me_3ImMe_3)]^+$ complex: at low scan rates the peak at $E_{pa}^{A}$ is observed, and at higher scan rates a shift of the equilibrium favors the appearance of $E_{pa}^{B}$. However, it does not allow the observation of the corresponding cathodic peak $E_{pc}^{B}$ for the reduction of the Cu(II) complex, indicating that this species is clearly unstable at the time scale of the experiment. The quasi-reversible process, observed at low scan rates corresponding to the potential at equilibrium, has thus skipped from $E^0_B$ for tris(pyridine) to the more negative of the microscopic processes $E^0_A = 0.00$ V. The parameters deduced from the fitting of the CVs (Figure 3d) attest the intuitive interpretation of the CVs concluding to a Cu(I) adaptable to a four- and five-coordinated geometry ($k_1 \cong k_{-1}$, $K_1 = 1.7$). Conversely, the Cu(II) complex shows a preferential stability for a five-coordinated SBP conformation ($K_2 = 4.1 \times 10^{-3}$) with a kinetic barrier for the SBP → Td rearrangement of the Cu(II) ($k_2 \ll k_{-2}$). This kinetic barrier orientates the mechanism toward the pathway "A" which is the classical route for copper complexes in an unconstrained environment (Scheme 5).

The set of CVs of the $[Cu^{I}(X_6tBu_3ImMe_3)]^+$ complex at different scan rates in MeCN appear completely different. It is similar for the other sterically hindered compounds, $R^1$ = Et, $R^2$ = Et, *i*Bu (Table 1). As shown in Figure 4a, the system at $E^0 = +0.10$ V ($\Delta E_p = 100$ mV at 0.1 V $s^{-1}$) remains reversible and almost unaffected by the scan rate. Hence, contrarily to the precedent case, the reorganization requires a very low activation energy. Indeed previous structural (XRD) and spectroscopic (NMR, EPR) studies have shown that, when tris(imidazole) compounds are sterically hindered, the geometry is generally enforced toward trigonal bipyramid (TBP) (Scheme 6).[19d,f] As emphasized in Schemes 3 and 4, this is explained by the fact that steric repulsion between the $-OR^1$ and $-NR^2$ groups

***Scheme 7.*** Proposed Redox Process for the $[Cu^{II}(X_6Me_3Pyr_3)]^{2+}$ Complex in MeCN

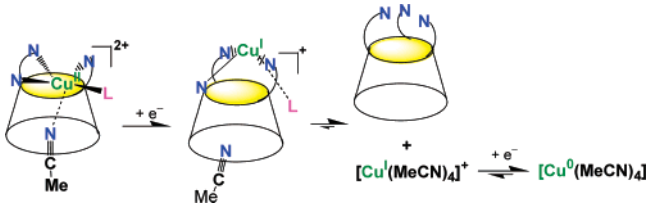

induces a flattened cone conformation in which the *t*Bu-phenoxyl units are strongly constrained in alternate *in* and *out* position relative to the cavity. Such a rigidified macrocyclic structure imposes a trigonal environment to the metal center with a relatively closed cavity entrapping MeCN. With bulky $-NR^2$ groups, a same conformation can also result from an equal effect on the other *t*Bu-phenoxyl groups. Thus, as depicted in Scheme 6, the best proposition for the mechanism of electron transfer for the bulky $OR^1ImR^2$ complexes is a pathway in which the reorganization remains limited to the exchange of an axial exogenous ligand, Cu(II) TBP ↔ Cu(I) TP (trigonal pyramid).[8] This is a very low-energy process. As a matter of fact, such mechanism can be considered as a process in which only one microscopic system of the square-scheme is at work, the topological reorganization remaining extremely limited.

Finally, for the tris(pyrrolidine) and tris(dimethylamine) Cu(II) complexes, only a totally irreversible cathodic peak is observed. Its intensity remains linear with $v^{1/2}$ (Figure 4b). Very low scan rates generate a redissolution Cu(0) peak, and higher scan rates produce an anodic peak at $E_{pa} = -0.2$ V, which is ascribed to the oxidation of a Cu(0) transiently stabilized decomposition species.[27] This observation leads to the conclusion that reduction of Cu(II) into Cu(I) in this complex involves a fast decoordination of the metal. This is corroborated by the failure to isolate the Cu(I) derivative by a synthetic procedure: it can be explained by the strong stabilization of the Cu(II) complex which renders the Cu(II)/Cu(I) redox potential so negative that it is impossible to generate a stable Cu(I) complex prior to the reduction of copper to the elemental stage.[3] By comparison with the two other families of Cu-$N_3$-calix[6]arene complexes, (i) the insensitivity of the CVs of the tris(amine) complexes to the effect of the presence of nitrile, (ii) the fact that strong electron donor N ligand weakens the Cu−nitrile interactions,[19d,f] and (iii) the parameters from the EPR data lead us to conclude that these Cu(II) complexes have a distorted four-coordinated SP geometry with very weak MeCN interactions which vanishes after reduction. It thus appears that the redox pathway for the tris(amine) complexes is best represented as in Scheme 7.

## Discussion

The Cu-$N_3$-calix[6]arene funnel complexes have demonstrated earlier their ability to reproduce Cu biosites in structural and spectroscopic terms.[19−21] Electrochemical studies of complexes with various substituted N ligands have been performed in different organic solvents. They unravel the diverse factors of the supramolecular organization of the coordination regulating the redox properties of these systems. The first observation was that the presence of MeCN, buried inside the cavity, is a

(27) Bond, A.; Khalifa, M. A. *Inorg. Chem.* **1987**, *26*, 413−420.

***Scheme 8.*** Supramolecular Concept of the "Shoetree" Molecule Ensuring the Overall Fixation of the Coordination at Every Stage of the Cu(II)/Cu(I) Reorganization Process

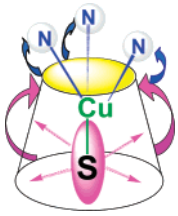


prerequisite for the quasi-reversible behavior in a dynamic mode for most of the complexes.[22] The second simple observation is that the stronger the electron-donating ability of the N ligand, the more negative is the Cu(II)/Cu(I) redox potential, which is an expected effect for the series: pyridine > benzimidazole > imidazole > diMeamine > pyrrolidine (Table 1). However, the complexity of the electrochemical behavior evidenced that the influence of the N ligand on the overall redox behavior was much more subtle.

The spectroscopic and structural properties have pointed out the importance of the entrapped MeCN molecule to stabilize a defined conformation for the calix[6]arene through weak CH$-\pi$ interactions between the methyl of the inner MeCN and the *t*Bu-phenoxyl of the calixarene cone. These properties largely support the electrochemical observations indicating that the presence of this guest ensures not only the fixed coordination of the two stable redox states, but as well and more importantly, a coherent host−guest interaction of the compound at the transient states during the reorganization process whether or not the metal remains coordinated to the nitrile (Scheme 2). Indeed, host−guest interactions between MeCN and calixarenes in the absence of metal have already been observed.[28] This proposition has been corroborated by the observation that when the calixarene cone is enlarged and opened, the CH$-\pi$ interactions are lowered, no more dynamic reversible behavior is observed. It thus appears that the crucial factor for the topological reorganization process is the structural role played by the MeCN guest molecule through CH$-\pi$ weak interactions to enforce a cone conformation. The transmission of the structuring forces by a bottom-up process from the cone through the N functions to the copper allows its conformational adaptability along the overall redox process.

This leads us to propose the supramolecular concept of a "shoetree" molecule (Scheme 8). Indeed this concept is quite equivalent to the "induced fit" biological process by which the functionality, here the redox dynamics, is reached through a responsive host/guest adaptation process.[16c]

This concept is largely corroborated by the comparative behavior of the tris(pyridine) and tris(imidazole) complexes. Their electrochemical study assisted by computational simulation has clearly highlighted that the redox process is under control of the dual-pathway square-scheme mechanism emphasized by Rorabacher as typical for the Cu(II)/Cu(I) systems. Remarkably, in the present study we have been able to establish that the route of electron transfer is controlled by the N ligand. Actually both pathways A and B (Scheme 5) are fully evidenced illustrating the dual gating of electron transfer.[3,7,8] Indeed, the strength of the Cu−nitrile interaction is function of the $\sigma$-donor character of the N ligand. Together with the CH$-\pi$ anchoring interactions of the inner MeCN, these two forces counterbalance to discriminate between preferential copper geometries. With the weaker donor pyridine, which adds a steric crowding on the upper rim, the anchoring interactions prevail and generate an inward supramolecular stress on the metal. This strongly favors the Td geometry at every stage of the redox process, even at the metastable Cu(II) state (Scheme 9). The electron transfer is thus favored through pathway B. This generates transiently a Td Cu(II) with an enhanced oxidizing power through route B (Scheme 5), as equalized to the more anodic microscopic potential $E^0_B$ ($E^0_B - E^0_A \cong 0.4$ V, Table 2), rationalizing the electrocatalytic oxidation of phenol by this derivative.[19b] Indeed, this observation corresponds to a definite entatic state as originally stated by Vallee and Williams.[8,11,15,16b]

With the stronger donating tris(imidazole) ligand, the Cu−$N_{Im}$ bond is strengthened and the Cu−nitrile interaction comparatively weakened. This allows the Cu(II) ion to relieve from the cavity inner stress and to impose to the system its preferential five-coordinated SBP geometry by interaction with an upper exogenous ligand (Scheme 9). Hence, in this case, the electron pathway is gated through the classical route A (Scheme 5). In turn, this determines the lowest of the microscopic redox potentials $E^0_A$ ($E^0_A \ll E^0_B$, Table 2). Actually, this complex displays a redox potential close to 0.0 V versus Fc, and no reactivity could be evidenced except reversible binding of CO by Cu(I).[19d] Hence, it appears clearly that in the framework of the square-scheme mechanism, the redox potential is not regulated only by the basicity of the ligand. The effective redox potential, in terms of oxidizing or reducing power toward the substrate, is also determined by the route of electron transfer, A or B, as it is then close to that of one of the microscopic redox processes, $E^0_A$ versus $E^0_B$, thus favoring, respectively, either a reduction or oxidation process (Scheme 5, Table 2).

Some of the derivatives of the tris(imidazole) family evidenced an alternative redox pathway indicating contrarily to the former complexes a weak energetic reorganization. Steric repulsion between the $-OR^1$ or $-NR^2$ substituents on the upper rim drives the three corresponding *t*Bu-phenoxyl groups into an *in* position which stabilizes $C_3$-symmetrical TBP/TP conformations (Schemes 6 and 9). As compared to the former, this does not influence the potential but was shown previously to enhance the stability of the CO adduct.[19d] This observation is an interesting illustration of a distant effect from the top to the bottom of the molecule. The entrapment of the inner ligand in the cavity in an axial configuration limits the reorganization process at the electron exchange to the binding of the exogenous upper axial ligand. This remote steric effect of the $-OR^1$ or $-NR^2$ groups of the calix host ligand, resulting in a control of the Cu(II)/Cu(I) process, appears remarkable as related to allosteric effects for substrate recognition and protein foldings.

Finally the tris(amine) family displayed another type of behavior. As emphasized by the electrochemical behavior, this ligand is a sufficient $\sigma$-donor to inhibit the effect of an inner Cu−nitrile bonding. This is proposed to favor an SP or SBP configuration as shown in Scheme 9. In combination with the strong donating effect of the N ligands, this specificity induces a very negative Cu(II) reduction potential. This disfavors

(28) (a) Arduini, A.; Giorgi, G.; Pochini, A.; Secchi, A.; Ugozzoli, F. *Tetrahedron* **2001**, *57*, 2411−2417. (b) Bonechi, C.; Donati, A.; Martini, S.; Rossi, C.; Arduini, A.; Pochini, A.; Lonetti, B.; Baglioni, P. *J. Phys. Chem. B* **2004**, *108*, 7603−7610.

***Scheme 9.*** Preferential Geometries Imposed by the Balance of the CH−$\pi$ Weak Interactions (Red Lines) and Electronic Forces (→) of the N Ligands: Supramolecular Control of the Cu Coordination in the Cu-$N_3$-Calix[6]arene Complexes in the Presence of MeCN

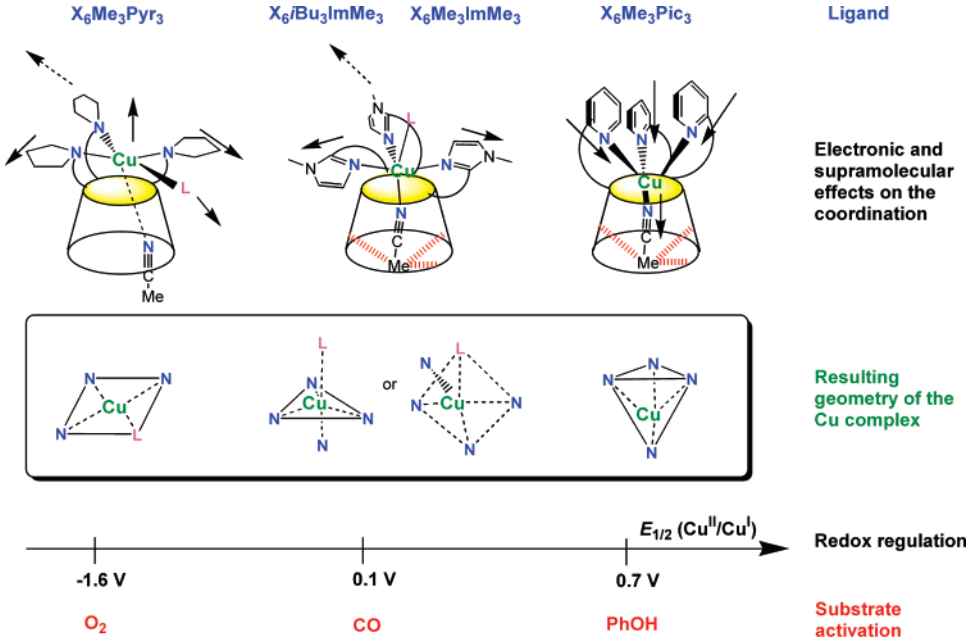


strongly the Cu(I) state for which the Td arrangement cannot be reached due to steric repulsion and to the absence of the inner nitrile. In turn, comparatively with the other complexes, this supports the high reactivity of the Cu(I) transient species toward $O_2$.[24]

## Conclusion

As outlined in the introduction of this work, the supramolecular control of the second coordination sphere of the Cu active site by the protein matrix is crucial for the orientation of the functionality of the Cu(II)/Cu(I)-based systems. Two major effects of the matrix are proposed to regulate this functionality: (i) constraints on the coordination of the metal as to regulate the electronic and, hence, redox properties and (ii) control of the host/guest interactions (molecular recognition) between the substrate and the hydrophobic proteic chamber (access channel and reaction site). Not so many low molecular weight synthetic systems have been developed so far as to reproduce these features for the sake of the understanding of these supramolecular regulating factors. The present electrochemical study of various substituted Cu-$N_3$-calix[6]arene complexes associated with voltammetric simulation, and supported by previous spectroscopic and structural characterization, demonstrates that these funnel complexes fulfill these specifications. Hence, they can be considered as exemplary supramolecular structural models for monocopper enzyme redox-active sites. Remarkably, the conception of these systems illustrates how the supramolecular organization of the coordination is connected to the regulation of the redox kinetics and thermodynamics and how this connection leads to preorganization for substrate activation (Scheme 9). The biological relevance with observation made on copper proteins for redox regulation by protein foldings is especially remarkable.[29] These observations are tangible evidence that the Cu(II)/Cu(I) process is an interesting probe for the understanding of the complex protein functionality, especially when Cu is surrounded by a hydrophobic patch controlling the secondary sphere.[2,3,15]

More generally, it is interesting to consider how the copper metal chemistry can be exploited through its electronic/geometric specificity in the duality of a "redox fuel" energetic machine: either as an energetic accumulator (entatic activation of substrates) when a structural stress is at work, as in the present case, or as a molecular motor, when the structural reorganization is free of constraint.[30]

## Experimental Section

**Synthesis.** According to the references cited in Table 1, the ligands were reacted with either 1 molar equiv of $[Cu(MeCN)_4]PF_6$ or $[Cu(H_2O)_n](Z)_2$ ($Z = ClO_4$ or $CF_3SO_3$) to produce a complex of general formulas $[Cu(X_6Me_3N_3)L]^+$ and $[Cu(X_6Me_3N_3)(H_2O)L]^{2+}$, respectively. In each case, the metal ion is coordinated to all three amino groups of the ligand and to an exogenous labile molecule L (which is either a solvent molecule, $H_2O$, or MeCN). The latter sits inside the calix[6]arene pocket and can be selectively exchanged for other small coordinating molecules.

**Synthesis and Characterization of $[Cu^{II}(X_6Me_3Pyr_3)(H_2O)_2](OTf)_2$, $[Cu^{I}(X_6Me_3Pyr_3)]PF_6$, and $[Cu^{II}(X_6Me_3Dmema_3)](OTf)_2$.** Under an inert anhydrous atmosphere ($N_2$ dry box), equimolecular quantities of the ligand $X_6Me_3Pyr_3$ (for synthesis and characterization, see ref 19h) and $Cu(OTf)_2$ were mixed in dry acetone to yield a green powder. After dissolution and filtration in THF, then precipitation by pentane, a light green product was obtained. Elemental analysis is in agreement with a general formula $[Cu^{II}(X_6Me_3Pyr_3)(H_2O)_2](OTf)_2$: calcd C 61.3, H 7.5, N 2.6; found C 61.1, H 7.25, N 2.82. Low-temperature EPR in $CH_3CN$ showed a spectrum with $g_{\|} = 2.23$ and $g_{\perp} = 2.05$ ($A_{\|} = 175$ G). A UV−vis d−d transition is observed at 680 nm ($\epsilon = 82$ $M^{-1}$ $cm^{-1}$). These features are typical of a cupric mononuclear complex in a square-based conformation. ES-MS spectra recorded either in MeCN or $CH_2Cl_2$ only displayed the parent peak

(29) (a) Winkler, J. R.; Wittung-Stafshede, P.; Leckner, J.; Malmström, B. G.; Gray, H. B. *Proc. Natl. Acad. Sci. U.S.A.* **1997**, *94*, 4246−4249. (b) Wittung-Stafshede, P.; Hill, M. G.; Gomez, E.; Di Bilio, A. J.; Karlsson, B. G.; Leckner, J.; Winkler, J. R.; Gray, H. B.; Malmström, B. G. *J. Biol. Inorg. Chem.* **1998**, *3*, 367−370.

(30) (a) Rhaem, L.; Sauvage, J.-P. *Struct. Bonding* **2001**, *99*, 55−78. (b) Kay, E. R.; Leigh, D. A.; Zerbetto, F. *Angew. Chem., Int. Ed.* **2007**, *46*, 72−191.

corresponding to the unmodified ligand. This observation likely arises from Cu(II) to Cu(I) reduction during the ionization process followed by a quick decomplexation. Any attempt to obtain crystals for X-ray characterization failed.

For the synthesis of the $[Cu^{I}(X_6Me_3Pyr_3)]PF_6$ compound, no pure product could be obtained. This is likely due to the poor coordinating ability of this ligand toward Cu(I) complexation. Nevertheless a product has been isolated from an equimolecular mixture of the ligand and $[Cu^{I}(MeCN)_4]PF_6$ in THF and precipitation by pentane in extremely inert and anhydrous conditions. This solid exhibits a mass peak $m/z = 1369$ corresponding to the expected cation $[Cu^{I}(X_6Me_3Pyr_3)]^+$ ($C_{87}H_{123}N_3O_6PF_6Cu$: mass, 1514). Contrarily to most of the other compounds of the $N_3$-calix[6]arene Cu(I) series, this compound revealed to be extremely sensitive toward $O_2$ and $H_2O$, which is indicative of a specific reactivity. It is noteworthy that after reaction with $O_2$ in the presence of traces of $H_2O$, a species with an EPR spectrum close to that observed for the isolated Cu(II) derivative was obtained. The $[Cu^{II}(X_6Me_3Dmema_3)](OTf)_2$ complex was synthesized as described above for the pyrrolidine derivative and exhibited similar spectroscopic parameters [$\lambda_{max} = 685$ nm in MeCN/THF, $g_{\|} = 2.26$ and $g_{\perp} = 2.06$ ($A_{\|} = 175$ G)].

**Electrochemistry.** The electrochemical studies of the copper complexes have been performed in a glovebox (Jacomex) ($O_2 < 1$ ppm, $H_2O < 1$ ppm) with a home-designed three-electrodes cell (WE, Pt; RE, Ag; CE, Cu). The potential of the cell was controlled by an AUTOLAB PGSTAT 100 (Ecochemie) potentiostat monitored by a computer. All solvents used ($CH_2Cl_2$, THF, MeCN, PhCN) have been distilled and kept under $N_2$. The supporting salt, $NBu_4PF_6$, has been purified, dried under vacuum for 48 h at 100 °C, then kept under $N_2$ in the glovebox. All experiments have been performed with solutions of $10^{-3}$ M in electroactive species. It has been checked that the behavior was not different for different values of concentration ($5 \times 10^{-4} \leq C \leq 3 \times 10^{-3}$ M). It has also been verified that the ligands are not electroactive in the selected domain; the free ligands and/or Zn complexes gave irreversible oxidation at potentials higher than +1.2 V. The experimentally measured ohmic drop (current interrupt method) was included in the simulation procedure as uncompensated solution resistance.

**Simulation Procedure.** The voltammograms have been simulated with a first-order reaction approximation. Although the coordination number of the studied compounds is not invariant during the electron-transfer process, the ligand exchange has been neglected in terms of kinetics and the conformational rearrangement considered as the limiting process. The fits have been performed with the Digisim 3.1 software using a double $C_{rev}E$ approximation as the reference mechanism (the electrochemical reactions are based on Butler−Volmer kinetics). The confidence level for all varying parameters is superior to 68.3%. Diffusion coefficients have been estimated at $2 \times 10^{-6}$ cm$^2$ s$^{-1}$. Surface area (0.024 cm$^2$) was determined by previous electrochemical experiments. The redox potentials in both geometries, $E^0_A$ and $E^0_B$, were extracted from the experimental CVs. Uncompensated resistance (100 Ω) and double-layer capacitance (0.8 $\mu$F) have been incorporated in the fits calculations. The best fits between the experimental and simulated sets of curves have been obtained for the tris(pyridine) and tris(imidazole) compounds when fixing, respectively, the symmetry coefficient α to 0.62 and 0.60 for the Cu(II)/Cu(I)$_{Td}$ system, 0.28 and 0.61 for the Cu(II)/Cu(I)$_{SBP}$ system. Preliminary simulations were performed to verify that the value of this parameter ($0.1 < \alpha < 0.9$) did not affect significantly the thermodynamic and kinetics $K$ and $k$ values. The "nonideal" values ($\neq 0.5$) obtained for α indicate that the reduction process is kinetically disfavored in the SBP geometry for the tris(pyridine) compound ($\alpha = 0.28$) and slightly favored for the tris(imidazole) compound ($\alpha = 0.61$). In the Td configuration ($\alpha = 0.62$ and 0.60), this process is also favored for both compounds. Particularly, the low value of $\alpha = 0.28$ describes a kinetically disfavored reduction process for the SBP complex. This may be due to the loss of the exogenous ligand from the Cu(II) species in the electron-transfer reaction (chemical step not included in the presented fitting model).

**Acknowledgment.** The authors acknowledge support from the CNRS, Conseil Régional de Bretagne (Doctoral fellowship for M.C.), and Conseil Général du Finistère (Postdoctoral fellowship for N.L.P.). Funds from Agence Nationale pour la Recherche (Calixzyme Project ANR-05-BLAN-0003) are acknowledged.

**Supporting Information Available:** Figure for the comparative behavior of the $[Cu^{I}(X_6Me_3Pic_3)]^+$ and $[Cu^{II}(X_6Me_3Pic_3)]^{2+}$ complexes in different solvents (MeCN, $CH_2Cl_2$, THF, and PhCN), figure for the behavior of the $[Cu^{I}(X_3Y_3Me_3Pic_3)]^+$ complex, figure for the $[Cu^{I}(X_6Me_3ImMe_3)]^+$ and $[Cu^{II}(X_6Me_3Pyr_3)]^{2+}$ complexes in the different solvents. This material is available free of charge via the Internet at http://pubs.acs.org.

JA071219H